THE EUROPEAN
PHYSICAL JOURNAL C

Reach and complementarity of $\mu \to e$ searches

Sacha Davidson[1,a], **Bertrand Echenard**[2,b]

[1] LUPM, CNRS, Université Montpellier, Place Eugene Bataillon, 34095 Montpellier Cedex 5, France
[2] California Institute of Technology, Pasadena, CA 91125, USA

Abstract In Effective Field Theory, we describe $\mu \leftrightarrow e$ flavour changing transitions using an operator basis motivated by experimental observables. This implies that $\mu \to e_L \gamma$, $\mu \to e_L \bar{e}e$ and $\mu \to e_L$ conversion on nuclei probe a six-dimensional subspace, where we derive constraints on the New Physics scale from past and future experiments, illustrating the complementarity of the processes in an intuitive way.

1 Introduction

Lepton flavor-violating contact interactions – referred to as LFV or CLFV – are excellent probes of physics beyond the standard model (see e.g. [1,2] for reviews). The non-zero neutrino masses and mixing angles imply their existence, and an observation could shed light on the neutrino mass mechanism [3], and even on the matter excess of our universe if generated via leptogenesis [4,5]. The rates could be just below the current experimental bounds, in many extensions of the Standard Model that introduce additional CLFV sources [2].

CLFV searches have been conducted in a wide range of reactions, and a subset of current and anticipated experimental constraints are given in Table 1. While the multitude of τ channels could contribute to identifying the nature of New Physics (NP), the greater sensitivity in muon sector seems more promising for discovering it. Although the number of muon processes is limited, the corresponding bounds are already quite restrictive, and exceptional improvements are expected in the coming years.

The reach and complementarity of $\mu \to e\gamma$, $\mu \to e\bar{e}e$ and $\mu A \to eA$ transitions have been explored from various perspectives. Numerous authors have investigated model

preferences and predictions for correlations among CLFV observables [20–30]. An early model-independent analysis was performed by de Gouvea and Vogel [31], using a simple effective Lagrangian to describe NP effects. The presentation of our results follows their intuitive plots. However, their approach was limited to comparing the reach of pairs of processes (e.g. $\mu \to e\gamma$ vs. $\mu A \to eA$) at tree level. More systematic Effective Field Theory (EFT) studies, including more operators and some loop effects, were performed in [32,33]; focused on the sensitivity of the processes to a more complete operator basis, and [33] explored whether the proposed experimental muon program is necessary and sufficient to find $\mu \to e$ flavour change.

The aim of this work is to graphically illustrate the complementarity and reach of the $\mu \to e\gamma$, $\mu \to e\bar{e}e$ and $\mu A \to eA$ processes. We describe the physics of CLFV in an EFT perspective [34–41], where the number of operator coefficients is reduced by choosing an operator basis motivated by our observables [33]. We quantify complementarity as the degree to which observables probe different operator coefficients, and study the complementarity of observables at the New Physics scale because the aim is to make observations that give distinct information at Λ_{LFV}. The coefficients are translated to Λ_{LFV} using Renormalisation Group Equations. This study extends the analysis described in [33] in several ways: we provide more informative plots of the current and projected experimental reaches, and a more rigorous construction of the basis for the subspace of experimentally accessible operator coefficients. In addition we draw attention to the information loss in matching nucleons to quarks using current theoretical results. Using this formalism to study whether $\mu \to e$ processes can distinguish among models is an interesting question that we leave for a subsequent publication.

This paper is organized as follows: Sect. 2 outlines the procedure to take the data parametrized in EFT from the experimental scale to beyond the weak scale. Section 3 presents constraints from various experimental measurements and

[a] e-mail: s.davidson@lupm.in2p3.fr (corresponding author)

[b] e-mail: echenard@caltech.edu

Table 1 Current bounds on the branching ratios for various lepton flavour changing processes, and the expected reach of upcoming experiments

Process	Current sensitivity	Future
$\mu \to e\gamma$	$< 4.2 \times 10^{-13}$ (MEG [6])	$\sim 10^{-14}$ (MEG II [7])
$\mu \to e\bar{e}e$	$< 1.0 \times 10^{-12}$ (SINDRUM [8])	$\sim 10^{-16}$ (Mu3e [9])
$\mu A \to eA$	$< 7 \times 10^{-13}$ (SINDRUM II [10,11])	$\sim 10^{-16}$ (COMET [12,13], Mu2e [14])
		$\sim 10^{-(18\to 20)}$ (PRISM/PRIME [15])
$\tau \to l\gamma$	$< 3.3 \times 10^{-8}$ (Babar) [16]	$\sim 10^{-9}$ (BelleII) [17]
$\tau \to 3l$	$< \text{few} \times 10^{-8}$ (Belle) [18]	$\sim 10^{-9}$ (BelleII) [17]
$\tau \to l\pi^0$	$< 8.0 \times 10^{-8}$ (Belle) [19]	$\sim 10^{-9}$ (BelleII) [17]
$\tau \to l\rho$	$< 1.2 \times 10^{-8}$ (Belle) [19]	$\sim 10^{-9}$ (BelleII) [17]

projections for future initiatives. The construction of the basis used in this work is discussed in Appendices A and C. An independent issue regarding information loss in relating $\mu A \to eA$ rates to models is finally discussed in Appendix B.

2 Theory overview

This section gives the Lagrangian and Branching Ratios at the experimental scale, and sketches the transformation of operator coefficients from the experimental scale to Λ_{LFV} (which is described in more detail in [33]).

A challenge of the EFT approach lies in the large number of operators. In the case of $\mu \to e$ flavour changing processes, about 90 operators [33] are required to parametrize interactions that have ≤ 4 Standard Model legs at low energy and are otherwise flavour-diagonal. The difficulty to constrain and visualize this high-dimensional space is compounded by the fact that there are (only) three processes with excellent sensitivity in the $\mu \to e$ sector (see Table 1), imposing only about a dozen constraints on operator coefficients [42]. Improved theoretical calculations and additional $\mu A \to eA$ measurements with different nuclear targets could increase this number to ~ 20 independent constraints [42]. Determining all EFT coefficients appears therefore a daunting task.

This manuscript takes a different perspective, following [33]. Since there are three processes with excellent experimental sensitivity, we restrict to the (12-dimensional) subspace of operator coefficients probed by $\mu \to e\gamma$, $\mu \to e\bar{e}e$, and Spin Independent[1] $\mu Al \to eAl$ and $\mu Au \to eAu$. The dimension of the subspace can be further reduced by half since the operator coefficients can be labelled by the helicity (or chirality) of the outgoing relativistic electron, and the results are very similar for either e_L or e_R, which do not inter-

fere. Restricting the analysis to the subspace corresponding to an outgoing e_L in the bilinear with a muon, the three muon processes can be described at the experimental scale ($\sim m_\mu$) by the following effective Lagrangian [1]:

$$\delta\mathcal{L} = \frac{1}{\Lambda_{LFV}^2}\Big[C_D(m_\mu \bar{e}\sigma^{\alpha\beta}P_R\mu)F_{\alpha\beta} + C_S(\bar{e}P_R\mu)(\bar{e}P_Re)$$
$$+ C_{VR}(\bar{e}\gamma^\alpha P_L\mu)(\bar{e}\gamma_\alpha P_Re)$$
$$+ C_{VL}(\bar{e}\gamma^\alpha P_L\mu)(\bar{e}\gamma_\alpha P_Le) + C_{Alight}\mathcal{O}_{Alight}$$
$$+ C_{Aheavy\perp}\mathcal{O}_{Aheavy\perp}\Big] \tag{2.1}$$

where Λ_{LFV} is the New Physics scale, and the dimensionless coefficients $\{C_Z\}$ are lined up in a vector $\vec{C}$ normalised to 1 at the experimental scale. The first term of this Lagrangian is a dipole operator mediating $\mu \to e\gamma$ and contributing to both $\mu \to e\bar{e}e$ and $\mu A \to eA$. The next three contact operators contribute to $\mu \to e\bar{e}e$, while $\mathcal{O}_{Alight}$ is a combination of operators probed by light muon conversion targets such as Ti or Al, and $\mathcal{O}_{Aheavy\perp}$ is an orthogonal combination probed by heavy targets such as Au. An Approximate expression for $\mathcal{O}_{Alight}$ at the experimental scale is given in Eq (A.2), and for $\mathcal{O}_{Alight}$ and $\mathcal{O}_{Aheavy\perp}$ at 2 GeV in Eq. (A.14). We take Au and Al as prototypical "heavy" and "light" targets since Au was used by the SINDRUM experiment [10,11], and Al will be used by the upcoming COMET [12,13] and Mu2e [14] experiments, in addition to resembling Ti used in the past [10,10].

The constraint on the dipole operator from $\mu \to e\gamma$ is given by:

$$BR(\mu \to e_L\gamma) = 384\pi^2 \frac{v^4}{\Lambda_{LFV}^4}|\vec{C}\cdot\hat{e}_{DR}|^2 < B_{\mu\to e\gamma}^{expt}$$
$$= 4.2 \times 10^{-13} \tag{2.2}$$

where we introduced unit vectors $\hat{e}_A$ which select coefficients C_A in the six-dimensional subspace. The four-lepton operators have negligeable interference in $\mu \to e\bar{e}e$ since the electrons are relativistic ($\approx$ chiral), setting the three follow-

---

[1] We leave Spin Dependent conversion [42,45,46] and other targets [42] for future work.

ing constraints:

$$BR(\mu \to e_L \overline{e_R} e_L) = \frac{v^4}{\Lambda_{LFV}^4} \frac{|\vec{C} \cdot \hat{e}_S|^2}{8} \leq B_{\mu \to e\bar{e}e}^{expt} = 10^{-12}$$

$$BR(\mu \to e_L \overline{e_L} e_L) = \frac{v^4}{\Lambda_{LFV}^4} \Big[2|\vec{C} \cdot \hat{e}_{VL} + 4e\vec{C} \cdot \hat{e}_D|^2$$
$$+ e^2(32 \ln \frac{m_\mu}{m_e} - 68)|\vec{C} \cdot \hat{e}_D|^2 \Big]$$
$$\leq B_{\mu \to e\bar{e}e}^{expt}$$

$$BR(\mu \to e_L \overline{e_R} e_R) = \frac{v^4}{\Lambda_{LFV}^4} \Big[|\vec{C} \cdot \hat{e}_{VR} + 4e\vec{C} \cdot \hat{e}_D|^2$$
$$+ e^2(32 \ln \frac{m_\mu}{m_e} - 68)|\vec{C} \cdot \hat{e}_D|^2 \Big]$$
$$\leq B_{\mu \to e\bar{e}e}^{expt}. \tag{2.3}$$

These can conveniently be summarised as

$$BR(\mu \to e_L \bar{e}e) = \frac{v^4}{\Lambda_{LFV}^4} \vec{C}^\dagger \boldsymbol{R}_{\mu \to e_L \bar{e}e} \vec{C} \leq B_{\mu \to e\bar{e}e}^{expt} \tag{2.4}$$

where the matrix $\boldsymbol{R}_{\mu \to e_L \bar{e}e}$ is proportional to the inverse covariance matrix for $\mu \to e\bar{e}e$, given in Eq. (A.4). Similarly, the Conversion Ratios for $\mu A \to eA$ can be written

$$CR(\mu\text{Al} \to e_L\text{Al}) = \frac{v^4}{\Lambda_{LFV}^4} \vec{C}^\dagger \boldsymbol{R}_{\mu\text{Al} \to e_L\text{Al}} \vec{C} \leq B_{\mu\text{Al} \to e\text{Al}}^{expt}$$

$$CR(\mu\text{Au} \to e_L\text{Au}) = \frac{v^4}{\Lambda_{LFV}^4} \vec{C}^\dagger \boldsymbol{R}_{\mu\text{Au} \to e_L\text{Au}} \vec{C}$$
$$\leq B_{\mu\text{Au} \to e\text{Au}}^{expt} \tag{2.5}$$

where the $\boldsymbol{R}$ matrices are given in Eq. (A.10). These expressions justify a posteriori the basis in Eq. (2.1), chosen to be orthogonal, intuitive, and correspond closely to the coefficient combinations probed by observables. The eigenvectors of the covariance matrix could be another basis choice, discussed briefly in Appendix C3.

From the Lagrangian (2.1), one can easily deduce that the three processes are complementary at the experimental scale: four-fermion interactions with leptons only contribute to $\mu \to e\bar{e}e$, interactions with strongly-interacting particles only contribute to $\mu A \to eA$ (the complementarity between heavy or light targets is discussed at the end of Appendix A), while the dipole contributes to all processes. The complementarity of two processes can be interpreted geometrically as the misalignment between the corresponding vectors in coefficient space, defined as the angle η between the two vectors. In terms of $\boldsymbol{R}$ matrices, the complementarity between processes A and B can be expressed as:

$$\cos^2 \eta \sim \frac{\text{Tr}\big[\boldsymbol{R}_A \boldsymbol{R}_B\big]}{\text{Tr}\big[\boldsymbol{R}_A\big]\text{Tr}\big[\boldsymbol{R}_B\big]}, \tag{2.6}$$

which vanishes for perfectly complementary observables, and is equal to one when they contain the same information. The basis in Eq. (2.1) was chosen to be perfectly complementary, i.e. orthogonal, at the experimental scale.

In the following, we adopt a different approach to illustrate the complementarity between processes. Instead of using the geometric measure defined above, we show that each process gives independent information about the operator coefficients by plotting the corresponding reach separately. The measured rates can then be combined to identify a point in parameter space.

The degree of complementarity can be evaluated at Λ_{LFV} by translating the coefficients in Eq. (2.1) from the experimental scale to Λ_{LFV}. Modifying the scale amounts to changing the separation between lower energy loop effects that are explicitly calculated, and higher energy loops that are implicitly resummed into the coupling constants. At the experimental scale, all the loops via which a New Physics model contributes to an observable are in the operator coefficients, and the rate is straightforward to calculate. On the other hand, the operator coefficients at the heavy LFV scale are easily derived from a New Physics model, but loops must be calculated to evaluate experimental quantities. So the low-energy operator coefficients of Eq. (2.1) can be transformed to the LFV scale Λ_{LFV} via the Renormalisation Group Equations (RGEs) [32,43,44], which peel off the SM loops in a leading log expansion. Solving the RGEs perturbatively, and modifying the EFT with scale to account for the changing particle content, allows us to write

$$\vec{C}(m_\mu) = \boldsymbol{G}^T(\Lambda_{LFV}, m_\mu)\vec{C}(\Lambda_{LFV}). \tag{2.7}$$

The matrix $\boldsymbol{G}$ is similar to that given in [33]. We neglect loop effects in the EFT of nucleons and pions and match at 2 GeV onto a QCD-invariant EFT with gluons and five flavours of quarks (see Appendix A and Table 4). The leading log QED and QCD effects are included up to m_W [32,47], where the coefficients are matched (at tree level in the lower-energy EFT) onto dimension six SMEFT operators, augmented by the dimension eight scalar operator [48,49] corresponding to $\hat{e}_S$, which could be relevant [50]. We neglected CKM angles in matching and some other relevant SMEFT operators of dimension eight, and stress that the running from $m_W \to \Lambda_{LFV}$ is not included.

The Branching Ratios in terms of coefficients at Λ_{LFV} can be expressed as:

$$BR(\mu \to e_L X) \tag{2.8}$$
$$= \vec{C}^\dagger(m_W)\boldsymbol{G}^*(m_W, m_\mu)\boldsymbol{R}_{\mu \to e_L X}(m_\mu)\boldsymbol{G}^T(m_W, m_\mu)$$
$$\times \vec{C}(m_W)$$

where the matrix $\boldsymbol{G}$ is *not* unitary, and does not preserve the orthonormality of the basis since SM loops and matching can change the normalisation and direction of the vec-

Fig. 1 Reach as a function of (left) the angle θ_D, which parametrizes the relative magnitude of dipole and four-fermion coefficients, and (right) the variable $\kappa_D = \cot an(\theta_D - \pi/2)$. The scale Λ is defined in Eq. (2.1) with the coefficients normalised according to Table 2. The solid region is currently excluded
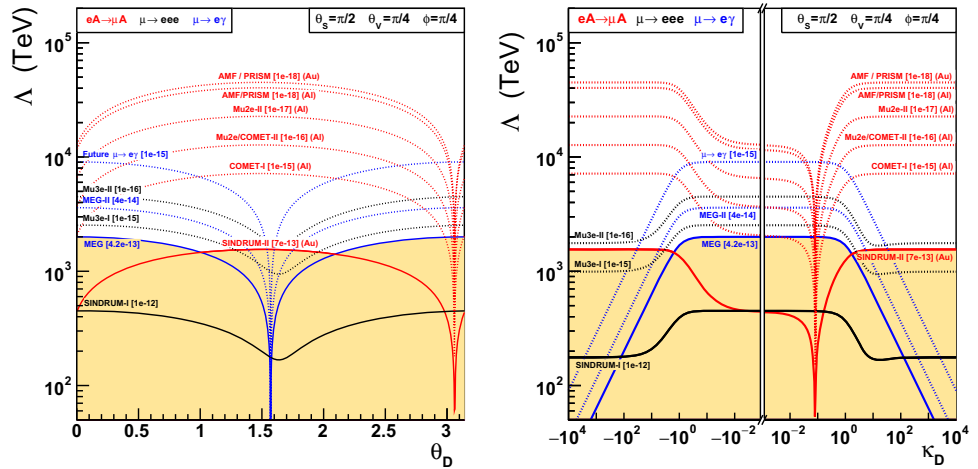
tors $\{\hat{e}_A\}$. This is expected since distinct observations at low energy can measure the same high-scale NP coefficients. The changing modulus of the basis vectors is simple to calculate and include, and affects the reach. The changes in direction can affect the complementarity of processes if the vectors become more or less aligned (see Appendix C).

3 Illustrating experimental constraints

In this section, we illustrate the constraints on New Physics from current and future $\mu \to e$ searches, and show how these results can be combined to identify the allowed region of coefficient space. We parametrize the coefficient space with spherical coordinates [51] (Table 2) assuming that the vector of coefficients $\vec{C}$ is normalised to unity at the experimental scale. The reach of the various experiments in Λ_{LFV} can be calculated as a function of these angles and the branching ratios given in Eq. C.3. We stress that we are showing (projected) exclusion curves, as opposed to "one-at-a-time" bounds, since our EFT formulation should account for potential cancellations in the theoretical rate.

In deriving this parametrization, we approximate the operator coefficients as real numbers. This familiar simplification reduces our coefficient space from six complex to six real dimensions, replacing relative phases between interfering coefficients with a relative sign. Furthermore, we focus on a four-dimensional subspace, corresponding approximately to the four processes we examine, by suppressing two of the three four-lepton directions (the four-lepton operators can be distinguished by measuring the angular distribution in $\mu \to e\bar{e}e$ [52,53]). The direction $\vec{e}_S$ associated to the scalar four lepton operator interferes with none of the other operators and receives negligible loop corrections, so it is complementary by inspection. We also neglect a linear combination of the vector four-lepton directions $\vec{e}_{VR}$ and $\vec{e}_{VL}$, since their contributions to $\mu \to e\bar{e}e$ have similar form. A judicious choice ensures the approximate orthogonality of

Table 2 Dimensionless operator coefficients expressed in the angular coordinates. The radial coordinate is $1/\Lambda_{LFV}^2$, $\theta_I : 0..\pi$ and $\phi : 0..2\pi$. As discussed in Appendix 1, the $\vec{e}_{VL} \times \vec{e}_{VR}$ plane was projected to a line, deviations from which are measured by θ_V. In general, the basis vectors $\{e_A\}$ are not unit vectors, and their normalisation is given in Table 5 and after Eq. (C.3) for the primed vectors

$\vec{C} \cdot \vec{e}_D$	$|\vec{e}_D| \cos \theta_D$
$\vec{C} \cdot \vec{e}_S$	$|\vec{e}_S| \sin \theta_D \cos \theta_S$
$\vec{C} \cdot \vec{e}_{VL}$	$|\vec{e}'_{VL}| \sin \theta_D \sin \theta_S \cos \theta_V$
$\vec{C} \cdot \vec{e}_{VR}$	$|\vec{e}'_{VR}| \sin \theta_D \sin \theta_S \cos \theta_V$
$\vec{C} \cdot \vec{e}_{Alight}$	$|\vec{e}_{Alight}| \sin \theta_D \sin \theta_S \sin \theta_V \sin \phi$
$\vec{C} \cdot \vec{e}_{Aheavy\perp}$	$|\vec{e}_{Aheavy\perp}| \sin \theta_D \sin \theta_S \sin \theta_V \cos \phi$

the remaining four basis vectors. The full details are given in Appendix C. Modulo these approximations, the parametrisation describes the experimentally constrainable space, so we now plot various slices through the excluded region to illustrate its shape.

We plot in Fig. 1 the reach of $\mu \to e_L\gamma$, $\mu \to e_L\bar{e}e$ and $\mu Al \to e_L Al$ as a function of θ_D for $\theta_S = \pi/2$, $\theta_V = \pi/4$, and $\phi = \pi/4$. This corresponds to $\vec{C} \cdot \vec{e}_S = 0$, so $\mu \to e\bar{e}e$ induced by the $\vec{C} \cdot \vec{e}_D$, $\vec{C} \cdot \vec{e}_{VR}$ and $\vec{C} \cdot \vec{e}_{VL}$, and $\mu A \to eA$ probed by Al and Au. At $\theta_D = 0$, the dipole coefficient is only contribution to the rates. At $\theta_D = \pi/2$, $\vec{C} \cdot \vec{e}_D$ vanishes (so does $\mu \to e\gamma$) and $\mu \to e\bar{e}e$ and $\mu A \to eA$ are purely mediated by four-fermion operators. For $\theta_D > \pi/2$, $\vec{C} \cdot \vec{e}_D$ is negative and $\mu A \to eA$ vanishes when the dipole contribution cancels the remaining contributions. The rate drops abruptly, indicating that the dipole contribution is relatively small and the cancellation only occurs in a narrow region. The valley is broader for $\mu \to e\bar{e}e$, since the contribution of $\vec{C} \cdot \vec{e}_D$ is more important, and the rate never vanishes because $\mu \to e\bar{e}e$ independently constrains each coefficient contributing to this process, so the rate only vanishes when all the coefficients do (see Eq. 2.3); although the dipole interferes with four-fermion contributions in the amplitude, the
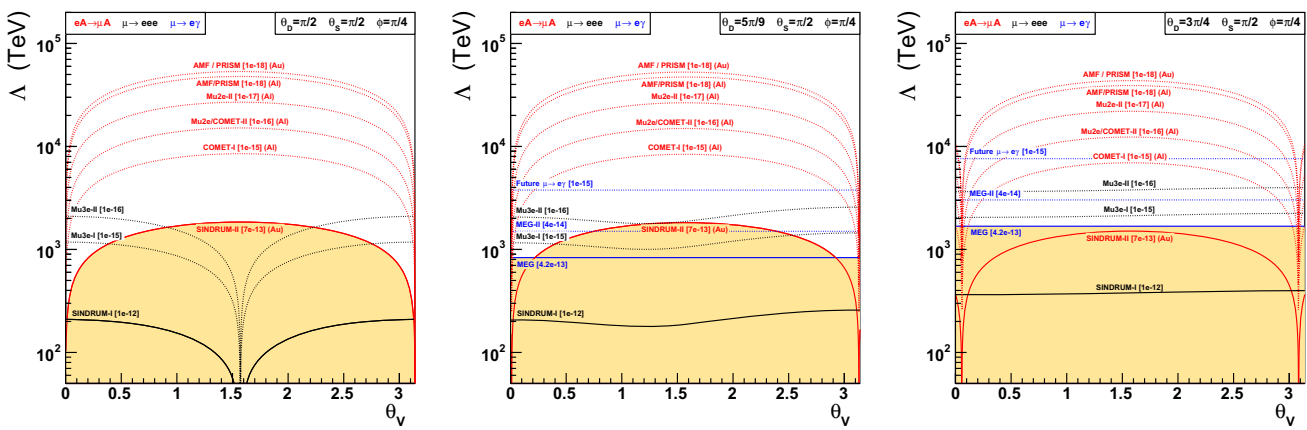
Fig. 2 Reach as a function of the angle θ_V, which is effectively the angle between the $\mu \to e\bar{e}e$ and $\mu A \to eA$ four-fermion operators, for different contributions of the dipole operator: (left) $\theta_D = \pi/2$, (middle) $\theta_D = 5\pi/9$, and (right) $\theta_D = 3\pi/4$. The solid region is currently excluded
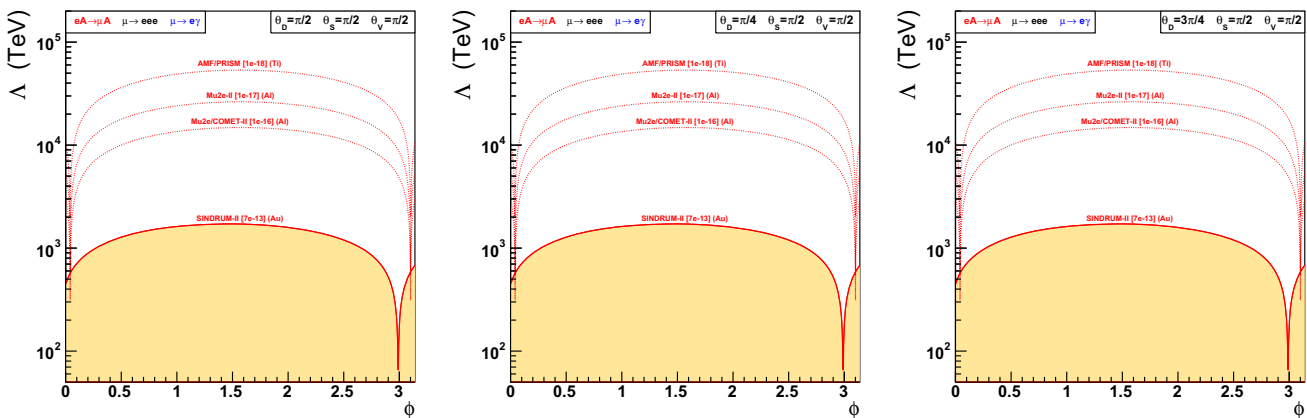

Fig. 3 Reach as a function of the angle ϕ for different contributions of the dipole operator: (left) $\theta_D = \pi/2$, (middle) $\theta_D = \pi/4$, and (right) $\theta_D = 3\pi/4$. Note that ϕ runs from $0 \to 2\pi$, although it is plotted from $0 \to \pi$; the rates for $\phi \in (\pi \to 2\pi)$ with positive dipole are equal to those with negative dipole and $\phi \in (0 \to \pi)$. The solid region is currently excluded

long-distance log enhancement of the dipole prevents the vector from cancelling it in the BR.

Our angular coordinate parametrisation defined a measure on the parameter space that assumes all the coefficients in our subspace are $\mathcal{O}(1)$ once the scale Λ_{LFV} is fixed. This might not be the case in some classes of models; for instance $\vec{C} \cdot \vec{e}_D \gg$ four-fermion coefficients can occur (in SUSY [54]), or the dipole could be suppressed, when the four-fermion operators are generated at tree level. To illustrate complementarity when the "natural" size of $\vec{C} \cdot \vec{e}_D$ is significantly different from the other coefficients, we also plot the reach in a parametrization similar to that introduced in [31] by defining a variable

$$\kappa_D = \cotan(\theta_D - \pi/2). \tag{3.1}$$

This non-linear transformation magnifies the regions where the dipole contribution either dominates the four-fermion interactions ($\theta = 0, \pi$) or is suppressed ($\theta = \pi/2$). (A similar variable $\kappa_V = \cotan(\theta_V)$ could be defined to magnify the

regions where leptonic four-fermion coefficients are much larger or smaller than those with quarks.) We subtract $\pi/2$ in Eq. (3.1) in order to have $\mu \to e\gamma$ larger at the centre of the plot[2] following [31].

Figure 2 displays the reach as a function of θ_V, which is effectively the angle between the $\mu \to e\bar{e}e$ and $\mu A \to eA$ four-fermion operators. Results for a vanishing dipole contribution ($\theta_D = \pi/2$) shows that $\mu \to e\bar{e}e$ vanishes at $\theta_V = \pi/2$ and $\mu A \to eA$ at $\theta_V = 0, \pi$. Adding a small negative dipole coefficient, $\mu \to e\bar{e}e$ doesn't vanish anymore since the dipole contributes independently as well as in interference with the four-fermion contributions, and the rate is reduced when this interference is destructive. The magnitude of the negative dipole coefficient is larger for $\theta_D = 3\pi/4$, exhibiting that $\mu A \to eA$ vanishes when the dipole cancels the four-fermion contributions.

---

[2] This choice means that $\kappa = 0$ corresponds to both to $\theta = 0$ and $\theta = \pi$, whereas $\pm\infty$ are identified. The plotted rates are not discontinuous at 0, because all the coefficients at $\theta = 0, \pi$ differ by a sign.
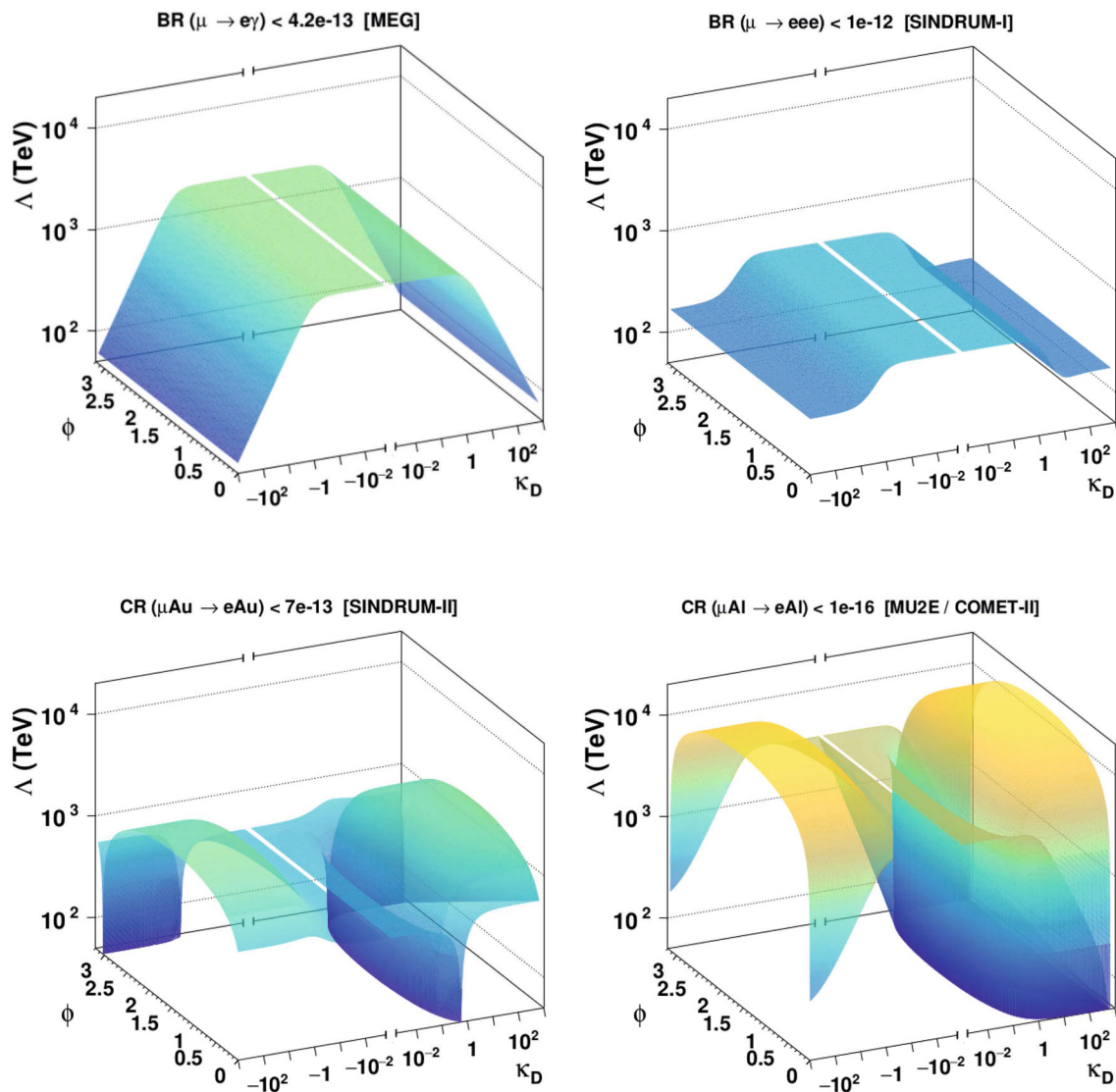
Fig. 4 Reach as a function of the angle ϕ and the variable κ_D for $\theta_V = \pi/4$ and $\theta_S = \pi/2$. Note that ϕ runs from $0 \to 2\pi$, although it is plotted from $0 \to \pi$; the rates for $\phi \in (\pi \to 2\pi)$ with positive dipole are equal to those with negative dipole and $\phi \in (0 \to \pi)$

Figure 3 illustrates the complementarity of heavy and light targets for $\mu A \to eA$, by plotting the conversion ratios as function of $\vec{C} \cdot \vec{e}_{Alight} \propto \sin\phi$ and $\vec{C} \cdot \vec{e}_{Aheavy\perp} \propto \cos\phi$. Recall that $\vec{C} \cdot \vec{e}_{Aheavy\perp}$ parametrizes the independent information obtained with Au. This additional contribution to $\mu Au \to e_L Au$ causes the rate to vanish at a different value than that of the light targets. The dipole, which also contributes to $\mu A \to eA$, was taken to either vanish ($\theta_D = \pi/2$), be positive ($\theta_D = 3\pi/4$) or negative ($\theta_D = \pi/4$). This illustrates the impact of $\vec{C} \cdot \vec{e}_D$ on the rate: cancellations can occur among the dipole and four-fermion contributions, as well as between the two independent combinations of four-fermion coefficients.

Finally, the dependence of the sensitivity on the angle ϕ and the variable κ_D is exhibited in Fig. 4. As expected, the $\mu \to e\gamma$ and $\mu \to e\bar{e}e$ processes are independent of ϕ. The shape of the conversion processes on light and heavy targets are globally similar, although the ridges along which the rates cancel are slightly different.

4 Summary

We use bottom-up EFT to calculate the reach and illustrate the complementarity of experiments searching for NP. This method is particularly well-suited to situations in which the number of observables is much smaller than the number of operators. It provides a complete parametrisation of the rates, without redundancies, and the EFT translation to Λ_{LFV} can be systematically improved. In addition, this formalism allows to explore the complementarity in a self-consistent

manner at the same scale at which the theory is defined, and ensure that experiments effectively probe different combinations of NP parameters. This approach is generic and can be applied to many situations. In this manuscript, we use it to study CLFV in the muon sector and derive sensitivity projections for current and future experiments.

At the experimental scale, the Lagrangian given in Eq. (2.1) includes all and only the operators contributing at tree level to the observables. The combinations of coefficients constrained experimentally define the operator basis for our subspace, whose dimension is equal to the number of constraints. For $\mu \to e_L \gamma$, $\mu \to e_L \bar{e}e$ and Spin Independent $\mu \text{Al} \to e_L \text{Al}$ and $\mu \text{Au} \to e_L \text{Au}$, this subspace is six-dimensional. These coefficients are translated to Λ_{NP} by solving the leading order Renormalisation Group Equations below the weak scale, and matching them to SMEFT at tree level (see Eq. (2.7)). Since the number of constraints remains unchanged, the dimension of the subspace cannot grow (but it could decrease, as discussed in appendix B). However, the normalisation and direction of the basis vectors is altered, in order to include, at Λ_{LFV}, the contributions from all the operators to the observables via short-distance effects described in the RGEs.

The ability of different experiments to probe independent operator coefficients – our definition of complementarity – is related to the misalignment between vector of coefficients. While it can be measured in various ways, we observe that a judiciously selected subset of our basis vectors remain approximately orthogonal above the weak scale, and we use various parametrisations (see Table 2 or Eq. (3.1)) to plot the experimental exclusion curves using the Branching Ratios given in Eq. (C.3). We also display a few projections to illustrate the reach and complementarity of future experiments.

An example of distinct observables probing the same New Physics is recalled in appendix B: $\mu A \to e A$ on various nuclei could distinguish scalar $\mu \to e$ contact interactions on neutrons from protons, but this may not allow the distinction of LFV scalar operators involving up quarks from those with down quarks. Improving the precision of the scalar $\bar{q}q$ expectation values in the nucleon would be required to improve the situation.

This work is only a preliminary implementation of bottom-up EFT, relying on theoretical formalism described in [33]. In future work, we aim to implement the Renormalisation Group running of our vectors above the weak scale (it was neglected here for simplicity and the lack of knowledge of Λ_{LFV}), and match models onto the "observable subspace" at Λ_{LFV}. We hope that finding robust distinctions among model predictions could be simplified by the reduced dimension of the subspace.

Appendix A: Operators, rates and R-matrices at low energy

The operators contributing at the experimental scale $\sim m_\mu$ to the tree level amplitudes for $\mu \to e_L \gamma$, $\mu \to e_L \bar{e}e$ and Spin Independent $\mu A \to e_L A$ are given in Eq. (2.1), where the $\mu A \to e A$ operators can be expanded on:

$$\mathcal{O}_{S,R}^{NN} = \bar{e} P_R \mu \overline{N} N \ , \ \ \mathcal{O}_{V,L}^{NN} = \bar{e} \gamma^\alpha P_L \mu \overline{N} \gamma_\alpha N \qquad (A.1)$$

where $N \in \{p, n\}$, and the list neglects subdominant operators such as $\bar{e} P_X \mu F F$ [74]. The operator $\mathcal{O}_{Alight}$ is approximatively

$$\mathcal{O}_{Alight} \propto \frac{1}{2}(\mathcal{O}_{S,R}^{nn} + \mathcal{O}_{S,R}^{pp} + \mathcal{O}_{V,L}^{nn} + \mathcal{O}_{V,L}^{pp}). \qquad (A.2)$$

The Branching Ratios (BRs) for the various processes can be expressed in terms of the operator coefficients $\vec{C}$ and the matrices **R**:

$$BR(\mu \to e_L \gamma) = \frac{v^4}{\Lambda_{LFV}^4} \vec{C}^\dagger \boldsymbol{R}_{\mu \to e_L \gamma} \vec{C} \qquad (A.3)$$

$$\Leftrightarrow \boldsymbol{R}_{\mu \to e_L \gamma}(m_\mu) = 384\pi^2 \frac{v^4}{\Lambda_{LFV}^4} \hat{e}_D \hat{e}_D^\dagger$$

where $v \simeq m_t$ is the Higgs vev, and $\vec{C} \cdot \hat{e}_D = C_D$. For $\mu \to e_L \bar{e}e$, the BRs given in the text can be written using:

$$\boldsymbol{R}_{\mu \to e_L \bar{e}e}(m_\mu) = \frac{v^4}{\Lambda_{LFV}^4} \begin{bmatrix} 2 & 0 & 0 & 8e \\ 0 & 1 & 0 & 4e \\ 0 & 0 & \frac{1}{8} & 0 \\ 8e & 4e & 0 & 8e^2(8\ln\frac{m_\mu}{m_e} - 11) \end{bmatrix} (A.4)$$

where **R** is given in the basis $(C_{VL}^{e\mu ee}, C_{VR}^{e\mu ee}, C_S^{e\mu ee}, C_D^{e\mu ee})$.

For $\mu A \to eA$, we consider the conversion ratios on prototypical heavy and light targets, taken to be Au and Al.[3] Following Kitano, Koike and Okada (KKO) [62], the Spin-Independent conversion rate can be written

$$
\begin{aligned}
\mathrm{CR}_{SI}(\mu A \to e_L A) = \frac{4m_\mu^5}{\Lambda_{LFV}^4 \Gamma_{capt}} \Big| C_{V,L}^{pp} V_A^{(p)} \\
+ C_{S,R}^{pp} S_A^{(p)} + C_{V,L}^{nn} V_A^{(n)} + C_{S,R}^{nn} S_A^{(n)} + C_{D,R} \frac{D_A}{4} \Big|^2
\end{aligned}
$$
(A.5)

where we use the nucleus(A)- and nucleon(N)-dependent "overlap integrals" $V_A^{(N)}$, $S_A^{(N)}$, D_A given by KKO [62],[4] and Γ_{cap} is the rate for the muon to transform to a neutrino by capture on the nucleus. Some relevant rates are [75]:

$$
\Gamma_{capt} = g_A^{cap} \times 10^6 \mathrm{s}^{-1} = \begin{Bmatrix} Al & 0.7054 \\ Ti & 2.59 \\ Au & 13.07 \end{Bmatrix} \times 10^6 \mathrm{s}^{-1}
$$
(A.6)

KKO observed that the overlap integrals were nucleus-dependent, and measurements of $\mu \to e$ conversion on different targets could be used to determine the operator coefficients. Reference [42] explored this issue quantitatively, and showed that with current uncertainties, Ti and Au give independent constraints. In this work, we are interested in a slightly different question: whether the observables give different constraints on New Physics heavier than m_μ and Λ_{QCD}, instead of understanding if they are independent. Unfortunately, there is "information loss" in matching nucleons onto quarks (see Sect. B), so we match the nucleon onto quark operators before constructing the **R**-matrices for $\mu Al \to e_L Al$ and $\mu Au \to e_L Au$.

Nucleon operators can be matched at 2 GeV onto light quark operators (see [33] for a basis) as

$$
\begin{aligned}
\langle N(P_f)|\bar{q}(x)\Gamma_O q(x)|N(P_i)\rangle \\
\simeq G_O^{N,q} \langle N(P_f)|\bar{N}(x)\Gamma_O N(x)|N(P_i)\rangle \\
= G_O^{N,q} \overline{u_N}(P_f)\Gamma_O u_N(P_i)e^{-i(P_f-P_i)x}.
\end{aligned}
$$

We also include the two-step matching of scalar b and c operators $(\bar{e}P_R\mu)(\bar{Q}Q)$ [71,76], first onto the gluon operator $(\bar{e}P_R\mu)GG$, then onto nucleons. As a result, the nucleon and

quark coefficients are related as

$$
C_{O,X}^{NN} = \sum_q G_O^{Nq} C_{O,X}^{qq},
$$
(A.7)

where $O \in \{S, V\}$ and the relevant Gs are given in Table 4. One can then define quark "overlap integrals" for target A as

$$
\begin{aligned}
I_{A,S}^q = G_S^{pq} S_A^p + G_S^{nq} S_A^n \\
I_{A,V}^q = G_V^{pq} V_A^p + G_V^{nq} V_A^n
\end{aligned}
$$
(A.8)

where in this work we use the EFT results [64] for $G_S^{N,q}$, which differ by $\sim 50\%$ from lattice results [63,67]. Assembling the quark overlap integrals for target A into a "target vector" $\vec{u}_A$:

$$
\vec{u}_A = (I_{A,S}^b, I_{A,S}^c, I_{A,S}^s, I_{A,S}^u, I_{A,S}^d, I_{A,V}^u, I_{A,V}^d),
$$
(A.9)

allows to write the Conversion Ratio as

$$
\begin{aligned}
\mathrm{CR}_{SI}(\mu A \to e_L A) = \frac{6144\pi^3 v^4}{2.197 g_A^{cap} \Lambda_{LFV}^4} \Big| \vec{u}_A \cdot \vec{C} + C_D \frac{D_A}{4} \Big|^2 \\
\equiv \vec{C}^\dagger \boldsymbol{R}_{\mu A \to e_L A} \vec{C}
\end{aligned}
$$
(A.10)

where g_A^{cap} is defined in Eq. (A.6), and D_A is the KKO overlap integral for the dipole [62]. So the **R**-matrix at a scale of 2 GeV is

$$
\begin{aligned}
\boldsymbol{R}_{\mu A \to e_L A} = \frac{6144\pi^3 v^4}{2.197 g_A^{cap} \Lambda_{LFV}^4} \Big(\vec{u}_A + \frac{D_A}{4}\hat{e}_D\Big) \\
\otimes \Big(\vec{u}_A + \frac{D_A}{4}\hat{e}_D\Big)^\dagger
\end{aligned}
$$
(A.11)

This translation of nucleon to quark operators neglects higher order QED and "strong interaction" effects between the experimental scale m_μ and 2 GeV: the QED running is small for the considered operators, and we did not include recent χPT results [60].

The prospects of distinguishing coefficients by using different targets depend on the misalignment between the target vectors, which can be quantified as an angle [42]:

$$
\vec{u}_{A_1} \cdot \vec{u}_{A_2} = |\vec{u}_{A_1}||\vec{u}_{A_2}|\cos\theta.
$$
(A.12)

In the quark operator basis at 2 GeV, this angle is given for various potential targets in Table 3. The angles are smaller than the misalignment angles in the nucleon operator basis[42] (see Figs. 6 and 7), because the scalar quark overlap integrals are larger than the vector integrals, and comparable for u and d quarks. In addition, there is currently a large discrepancy, $\sim 50\%$, between lattice and EFT determinations of the scalar overlap integrals. We assume that this theoretical discrepancy can be solved, so that $\mu A \to e_L A$ on Au and Al give independent information.

Equation (A.11) gives the **R**-matrices for Al and Au, which probe directions in quark coefficient space that are misaligned by ~ 5 degrees, at a scale of 2 GeV. In the plane spanned by $\vec{u}_{Au}$ and $\vec{u}_{Al}$, the orthogonal combinations used

---

[3] SINDRUM searched for $\mu \to e$ conversion on Titanium [10,11], and we will use these results in our study. However, according to [42], Ti and Al probe the "same" operator coefficients within current uncertainties, so we will apply the Ti bounds along the direction in coefficient space corresponding to Al.

[4] The "$4/\Lambda_{LFV}^4$" in Eq. (A.5) differs from the "$2G_F^2$" given in KKO's Equation (14), because $-4\widetilde{C}|_{here} = \tilde{g}|_{KKO}$ in the case of four-fermion operators; and D_A is divided by 4 in the above because the dipole normalisation here is identical to KKO. In addition, the KKO overlap integrals are in units of $m_\mu^{3/2}$, which here sits in front.

Table 3 Misalignment angles (in degrees), between target vectors expressed in the quark operator basis

	Li	Al	Ti	Cu	Au	Pb
Li	–	0.545	0.714	1.06	5.57	6.69
Al		–	0.433	0.760	5.34	6.46
Ti			–	0.356	4.94	6.06
Cu				–	4.59	5.71
Au					–	1.12

in Eq. (2.1), can be obtained by writing the target vector $\vec{u}_{Au}$ for Au as:

$$\vec{u}_{Au} = |\vec{u}_{Au}|(\cos\theta_{AuAl}\hat{u}_{Al} + \sin\theta_{AuAl}\hat{u}_\perp) \Rightarrow \hat{u}_\perp$$
$$= \frac{\hat{u}_{Au} - \cos\theta_{AuAl}\hat{u}_{Al}}{\sin\theta_{AuAl}} \tag{A.13}$$

where θ_{AuAl} is given in Table 3, and $\vec{u}_\perp \approx .56\hat{e}_V^{uu} + .8\hat{e}_V^{dd}$ is the direction in coefficient space corresponding to the operator $\mathcal{O}_{Aheavy\perp}$ of Eq. (2.1). As a result, from Eqs. (A.2), (A.10) and Eq. (A.13), one approximatively obtains

$$\mathcal{O}_{Alight} \approx \frac{1}{\sqrt{2}}(\mathcal{O}_S^{uu} + \mathcal{O}_S^{dd}) + \frac{1}{16}(\mathcal{O}_V^{uu} + \mathcal{O}_V^{dd})$$
$$\mathcal{O}_{Aheavy\perp} \approx \frac{3}{5}\mathcal{O}_V^{uu} + \frac{4}{5}\mathcal{O}_V^{dd}. \tag{A.14}$$

Appendix B: Are scalar quark currents indistinguishable?

This Appendix is focused on the information loss that occurs in matching nucleons to quarks at 2 GeV. In the data, LFV scalar interactions with neutrons might be distinguishable from those on protons [42]. But current theoretical translations of the nucleon results to quarks erase any distinction between LFV interactions with scalar u or d currents (the subdominant s, c, b, t quarks are neglected in this section).

The Spin-Independent Conversion Rate (CR) is given in Eq. (A.5) in terms of operator coefficients on nucleons. This result is at "Leading Order" in the low energy theory, and does not include the next order in χPT (parametrically $\sim$ 10%, two-nucleon effects, pion exchange...) or in the nuclear matrix element. Such effects have been calculated for WIMP scattering [57,58], and some partial results for $\mu A \rightarrow eA$ have been obtained [59–61]. Improvements of the theoretical calculation of $\Gamma(\mu A \rightarrow eA)$ could change the form of the conversion ratio (this occurs in [60]), or reduce the uncertainties on its parameters, thereby resolving the issue discussed here.

To set the stage, recall from KKO [62] that the overlap integrals for scalar and vector densities of neutrons and protons differ by less than a factor of three. In particular, Al

approximately probes

$$C_{S,R}^{pp} + C_{V,L}^{pp} + C_{S,R}^{nn} + C_{V,L}^{nn}, \tag{B.1}$$

(neglecting the dipole which could be constrained/measured elsewhere). In addition, it was pointed out in [42] that measuring $\mu A \rightarrow eA$ on another light target with different numbers of n and p would allow the measurement of

$$C_{S,R}^{pp} + C_{V,L}^{pp} - C_{S,R}^{nn} - C_{V,L}^{nn}. \tag{B.2}$$

Then, as noted by KKO, vector overlap integrals dominate over the scalars in heavy targets, so comparing Al to Au could allow to determine

$$C_{S,R}^{pp} - C_{V,L}^{pp} + C_{S,R}^{nn} - C_{V,L}^{nn}. \tag{B.3}$$

However, heavy targets also have more neutrons, so the $n - p$ measurement from comparing two light targets is required to extract the $S-V$ from heavy targets. The one remaining combination of coefficients (an isospin-violating V-S difference) has little impact on the CR given in Eq. (A.5), and cannot be extracted with current theoretical uncertainties [42].

The operator coefficients on nucleons can be transformed to coefficients on quarks according to Eq. (A.7), using the matrix G given in Table 4.[5] Focusing on the first generation valence quarks, this can be written as:

$$\begin{pmatrix} C_{V,L}^{pp} \\ C_{V,L}^{nn} \\ C_{S,R}^{pp} \\ C_{S,R}^{nn} \end{pmatrix} = \begin{bmatrix} 2 & 1 & 0 & 0 \\ 1 & 2 & 0 & 0 \\ 0 & 0 & G_S^{pu} & G_S^{pd} \\ 0 & 0 & G_S^{nu} & G_S^{nd} \end{bmatrix} \begin{pmatrix} C_{V,L}^{uu} \\ C_{V,L}^{dd} \\ C_{S,R}^{uu} \\ C_{S,R}^{dd} \end{pmatrix} \tag{B.4}$$

where the vector coefficients exhibit the expected dominance of u quarks in the proton, and d quarks in the neutron: the quark vector coefficients can be calculated from the nucleon vector nucleon coefficients, and vice versa. In the case of the scalar coefficients, this is almost not the case; for both lattice and EFT determinations of the $G_S^{N,q}$, the determinant of the scalar submatrix in Eq. (B.4) is small compared to the product of two $G_S^{N,q}$ ($G_S^{pu}G_S^{nd} - G_S^{pd}G_S^{nu} \sim 9^2 - 8^2(6^2 - 5^2)$), causing large uncertainties when it is inverted to solve for quark coefficients as a function of nucleon coefficients. In addition,

---

[5] This transition to quarks was not included in [42] due to the discrepancy among theoretical determinations of the $G_S^{N,q}$.

Table 4 Expectation values of vector and scalar quark currents in the nucleon; the scalar values are sometimes called f_q^N [63], and for light quarks are related to $\sigma_{\pi N}$ [64], where $G_S^{N,q} = \frac{m_N}{m_q} f_q^N = \sigma_{\pi N}/m_q +$ isospin corrections. The first scalar G_S induced by u and d quarks were obtained via dispersive techniques [64–66] and EFT methods [69] (Some lattice calculations give similar results [70]). The second $G_S^{N,q}$ [in brackets] are the lattice results of BMW [67], and an average of lattice results [68] is used for the strange quark. The heavy quark scalar G_S are from the lattice [63], and in parentheses from [71]. In all cases, the $\overline{\text{MS}}$ quark masses at $\mu = 2$ GeV are taken as $m_u = 2.2$ MeV, $m_d = 4.7$ MeV, and $m_s = 96$ MeV [72]. The running heavy quark masses are [73] $m_c(m_c) = 1.27$ GeV, $m_b(m_b) = 4.18$ GeV. The nucleon masses are $m_p = 938$ MeV and $m_n = 939.6$ MeV

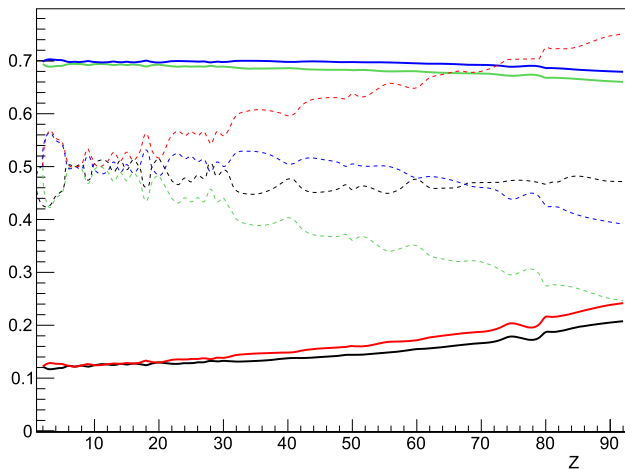| $G_V^{p,u} = G_V^{n,d} = 2$	$G_V^{p,d} = G_V^{n,u} = 1$	$G_V^{p,s} = G_V^{n,s} = 0$
$G_S^{p,u} = \frac{m_p}{m_u} 0.021(2) = 9.0$	$G_S^{p,d} = \frac{m_p}{m_d} 0.041(3) = 8.2$	
$\left[G_S^{p,u} = \frac{m_p}{m_u} 0.0139(13)(12) = 5.9 \right]$	$\left[G_S^{p,d} = \frac{m_p}{m_d} 0.0253(28)(24) = 5.0 \right]$	$G_S^{p,s} = \frac{m_N}{m_s} 0.043(11) = 0.42$
$G_S^{n,u} = \frac{m_n}{m_u} 0.019(2) = 8.1$	$G_S^{n,d} = \frac{m_n}{m_d} 0.045(3) = 9.0$	
$\left[G_S^{n,u} = \frac{m_n}{m_u} 0.0116(13)(11) = 5.0 \right]$	$\left[G_S^{n,d} = \frac{m_n}{m_d} 0.0302(3) = 6.0 \right]$	$G_S^{n,s} = \frac{m_N}{m_s} 0.043(11) = 0.42$
		$G_S^{N,c} = 0.0543 \left(= \frac{2m_N}{27m_c} f_{GG}^N \right)$
		$G_S^{N,b} = 0.0158 \left(= \frac{2m_N}{27m_b} f_{GG}^N \right)$

Fig. 5 Normalised quark (solid line) and nucleon (dotted line) overlap integrals as a function of the target charge Z. From the top-down at $Z = 90$: vector n (red, dotted), scalar d (blue) and u (green), vector p (black, dotted), scalar n (blue, dotted) and p (green, dotted), and vector d (red) and u (black). The nucleon overlap integrals are defined in Eq. (A.5), and those for quarks in Eq. (A.8); an overlap integral for nucleons (or quarks) in target A is normalised by dividing by the the square root of the sum of the squares of all the nucleon (or quark) integrals for that target

$G_S^{N,q} \gg G_V^{N,q}$ increases the sensitivity to scalar coefficients, and reduces the relative contribution of the vector coefficients to about the magnitude of the scalar uncertainties.

The effects of transforming from nucleon operators to quark operators can be seen in Fig. 5, where are plotted the quark and nucleon overlap integrals. This illustrates the difficulty to distinguish scalar u vs d, and also that the variation with Z is reduced for the quarks compared to nucleons.

The ability of different targets to distinguish among operator coefficients can be quantified as the angle between the directions they probe in coefficient space [42], where the direction is given by the overlap integrals for the target. Figs. 6 and 7 plots this misalignment angle as a function

of Z for various past and future targets. The plot on the left is for quark coefficients, and on the right is for nucleon coefficients (notice the difference in the vertical scale). Reference [42] estimated that a misalignment angle $\gtrsim 0.1$ was required to overcome theoretical uncertainties in the nuclear calculation, and obtain independent measurement of distinct nucleon operator coefficients. Even if one neglects the theoretical uncertainty in the $G_O^{N,q}$s, applying this $\gtrsim 0.1$ rule for quark coefficients suggests that the theoretical accuracy needs to be improved.

In summary, upcoming experiments could hope to bound or measure the three combinations of nucleon coefficients given in Eqs. (B.1–B.3). However, due to the almost-vanishing scalar determinant in Eq. (B.4), theoretical progress in calculating the G_S^{Nq} is required, for these to constrain three independent combinations of quark operator coefficients.

Appendix C: Including the penguin

This Appendix discusses the orthogonality of the basis used for the experimentally accessible subspace. We need an orthogonal basis to illustrate complementarity in polar coordinates; orthogonality would not be required to evaluate complementarity via Eq. (2.6), nor for exploring the model predictions for coefficients in the subspace. In the following, the term "penguins" refer to the operators of Eq. (C.1).

The basis vectors at $\Lambda_{LFV} \gtrsim m_W$ are $\mathbf{G}^*(m_W, m_\mu)\hat{e}_A$; we do not give explicit expressions because the translation from the observable-motivated basis to an arbitrary other choice is a technicality more suitable to computers. Expressions for various $\vec{C}^\dagger \mathbf{G}^*(m_W, m_\mu)\hat{e}_A$, appropriate for calculating LFV BRs in terms of coefficients at the weak scale, can be found in [33]. The norms and inner products among some basis
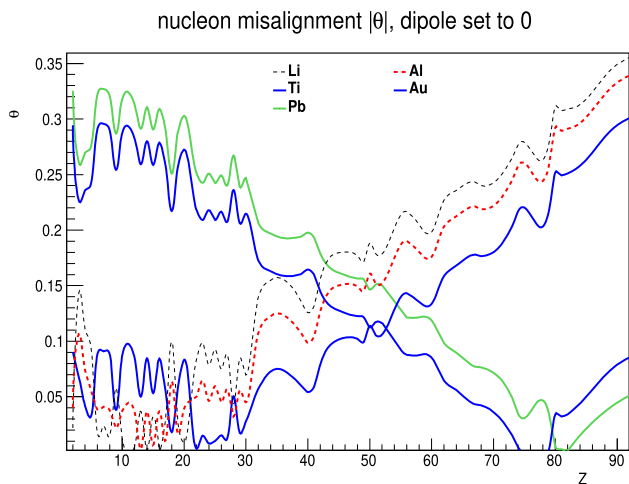
nucleon misalignment |θ|, dipole set to 0

Fig. 6 The misalignement angle θ (defined in Eq. (A.12)) between nucleon target vectors. The decreasing lines are lead (green, upper) and Au (blue); the rising lines are titanium (blue) and Al (red, dashed, middle) and lithium (black, dashed, upper)
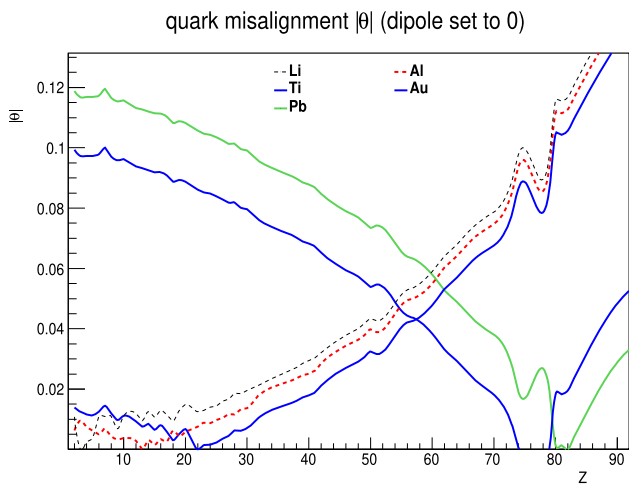
quark misalignment |θ| (dipole set to 0)

Fig. 7 The misalignement angle θ (defined in Eq. (A.12)) between quark target vectors; notice the reduced vertical scale and smoother lines as compared to the nucleon plot. The decreasing lines are lead (green, upper) and Au (blue); the rising lines are titanium (blue) and Al (red, dashed, middle) and lithium (black, dashed, upper)

vectors are given in Table 5, which shows an overlap of $10 \to 20$ degrees between the vector operators ($e_\perp$ has significant quark-vector components). The shrinking of the quark target-vectors is largely due to the shrinking scalar coefficients.

The overlap among the coefficients of $(\bar{e}\gamma^\alpha P_L \mu)(\bar{f}\gamma_\alpha f)$ operators arises because the $\mu \to e$ penguin operators of the SM EFT [77,78]:

$$\delta \mathcal{L}_{penguin} = \frac{C_{HL1}}{\Lambda_{LFV}^2}(\bar{\ell}_e \gamma^\alpha \ell_\mu)(H^\dagger \overset{\leftrightarrow}{D_\alpha} H)$$
$$+ \frac{C_{HL3}}{\Lambda_{LFV}^2}(\bar{\ell}_e \tau^a \gamma^\alpha \ell_\mu)(H^\dagger \overset{\leftrightarrow}{D_\alpha^a} H) \quad (C.1)$$

generate a flavour-changing vertex $\frac{gv^2}{c_W \Lambda_{LFV}^2}(C_{HL1}^{e\mu} + C_{HL3}^{e\mu})$ $\bar{e}\not{Z}P_L\mu$, so that Z exchange gives four-fermion operators in the low energy EFT:

$$\delta \mathcal{L} = \sum_{f,X} \frac{g_X^f (C_{HL1}^{e\mu} + C_{HL3}^{e\mu})}{\Lambda_{LFV}^2}(\bar{e}\gamma^\alpha P_L \mu)(\bar{f}\gamma^\alpha P_X f) \quad (C.2)$$

where f is any light chiral fermion, we used the SM Z interaction $\frac{g}{2c_W}(g_L^f P_L + g_R^f P_R)$ and $c_W = \cos\theta_W$. As a result, at the weak scale, the basis vectors $\vec{e}_{VL}$ and $\vec{e}_{VR}$ have components g_L^e and g_R^e in the two penguin directions, respectively, giving a tree-level contribution to $\vec{e}_{VL} \cdot \vec{e}_{VR}$ of order $2g_L^e g_R^e = 4s_W^2(-1 + 2s_W^2)$.

A more orthogonal basis could be obtained by removing the penguin contribution from the low energy $(\bar{e}\gamma^\alpha P_L \mu)$ $(\bar{f}\gamma_\alpha f)$ operators, and adding $Z \to \mu e_L$ as an observable at m_W. This is analogous to what was already done for the dipole, removing it from the combination of operators contributing to $\mu A \to e A$, and including $\mu \to e\gamma$ as an observable. However, this adds a dimension to the subspace, and tangles the intuitive link between basis vectors and observables. It is pursued in (C.2). (C.1) describes a simpler approach used to make the plots in the body of the paper.

C.1 A reduced basis at $\Lambda_{LFV} \sim m_W$

In this section we outline a method for choosing a penguin-less basis vector corresponding to a linear combination of $\vec{e}_{VL}$ and $\vec{e}_{VR}$, which is approximately orthogonal to the remaining basis vectors. In addition, the complementarity plots involving $\vec{e}_{VL}$ or $\vec{e}_{VR}$ are similar, so this choice suppresses redundancy.

The dependence of BR($\mu \to e\bar{e}e$) on C_{VL} and C_{VR} is very similar, as can be seen from Eq. (2.3). Since these coefficients can be distinguished via the angular distributions of the final state electrons in $\mu \to e\bar{e}e$ [52,53] rather than by comparing BR($\mu \to e\gamma$) and BR($\mu \to e\bar{e}e$), it is sufficient to plot $\mu \to e\gamma$ and $\mu \to e\bar{e}e$ in terms of a combination of these coefficients. By choosing this combination to suppress penguin contribution, we obtain five approximately orthogonal basis vectors.

As mentioned above, in the SMEFT basis at m_W, $\vec{e}_{VL}$ and $\vec{e}_{VR}$ have components $\sim g_L^e, g_R^e$ along the directions of the penguin operators of Eq. (C.1). So introducing $\vec{e}_V \propto g_R^e \vec{e}_{VL} - g_L^e \vec{e}_{VR}$, one sees that its penguin component vanishes at tree level, and $\vec{e}_V$ will be orthogonal to $\vec{e}_{Aheavy\perp}$ up to loop effects. We therefore replace the $\vec{e}_{VR} \otimes \vec{e}_{VL}$ plane by an axis along $\vec{e}_V$ and plot the complementarity of the three rates in the resulting 5-dimensional space.

In this reduced basis, the BRs can be written in terms of operator coefficients at $\Lambda_{LFV} \sim m_W$ as

$$\text{BR}(\mu \to e_L \gamma) = 384\pi^2 \frac{v^4}{\Lambda_{LFV}^4} \left[|\vec{e}_D|\cos\theta_D\right]^2$$

Table 5 Inner products between the basis vectors $\vec{e}_i(\Lambda_{LFV} \sim m_W) = G^*(m_W, m_\mu)\hat{e}_i$. On the diagonal are the norms (at m_W in SMEFT, for unit-normalised $\hat{e}_i$ at low energy), whereas the off-diagonals are $\cos\eta$, where η is the angle between the vectors. Overlaps smaller than 10^{-3} are given as 0

	$\vec{e}_{Alight}$	$\vec{e}_{Aheavy\perp}$	$\vec{e}_{VL}$	$\vec{e}_{VR}$	$\vec{e}_S$	$\vec{e}_D$
$\vec{e}_{Alight}$	0.768	0.05	0.022	-0.018	0	0
$\vec{e}_{Aheavy\perp}$		0.891	0.16	-0.14	0	0
$\vec{e}_{VL}$			1.13	-0.354	0	0
$\vec{e}_{VR}$				1.29	0	0
$\vec{e}_S$					1.00	0
$\vec{e}_D$						1.39

$$\text{BR}(\mu \to e\bar{e}e) = \frac{v^4}{\Lambda_{LFV}^4}\left[\frac{|\vec{e}_S|^2 \sin^2\theta_D \cos^2\theta_S}{8}\right.$$
$$+(|\vec{e}'_{VR}|\sin\theta_D\sin\theta_S\cos\theta_V + 4e|\vec{e}_D|\cos\theta_D)^2$$
$$+2(|\vec{e}'_{VL}|\sin\theta_D\sin\theta_S\cos\theta_V + 4e|\vec{e}_D|\cos\theta_D)^2$$
$$\left. +18.76(|\vec{e}_D|\cos\theta_D)^2\right]$$

$$\text{BR}(\mu Al \to eAl) = \frac{6144\pi^3 v^4}{2.197 g_{Al}^{cap}\Lambda_{LFV}^4}$$
$$\times \left[|\vec{u}_{Al}||\vec{e}_{Al}|\sin\theta_D\sin\theta_S\sin\theta_V\sin\phi + \frac{D_{Al}}{4}|\vec{e}_D|\cos\theta_D\right]^2$$

$$\text{BR}(\mu Au \to eAu) = \frac{6144\pi^3 v^4}{2.197 g_{Au}^{cap}\Lambda_{LFV}^4}$$
$$\times \left[|\vec{u}_{Au}|(\cos\theta_{AuAl}|\vec{e}_{Al}|\sin\theta_D\sin\theta_S\sin\theta_V\sin\phi \right.$$
$$\left. + \sin\theta_{AuAl}|\vec{e}_\perp|\sin\theta_D\sin\theta_S\sin\theta_V\cos\phi) + \frac{D_{Au}}{4}|\vec{e}_D|\cos\theta_D\right]^2$$
$$\text{(C.3)}$$

where we replace $\{\theta_{VR}, \theta_{VL}\} \to \theta_V$, the un-primed norms of the basis vectors at m_W are on the diagonal of Table 5 and $|\vec{e}'_{VR}| = -g_L^e|\vec{e}_{VR}|/\sqrt{(g_L^e)^2 + (g_R^e)^2} = 1.05$, $|\vec{e}'_{VL}| = g_L^e|\vec{e}_{VL}|/\sqrt{(g_R^e)^2 + (g_R^e)^2} = 0.709$, θ_{AuAl} is in Table 3, and norms obtained from the $\mu A \to eA$ overlap integrals and nucleon-quark matching are $|\vec{u}_{Al}| = 0.39706$ $|\vec{u}_{Ti}| = 0.991275$, and $|\vec{u}_{Au}| = 1.92876$.

C.2 An enlarged basis at $\Lambda_{LFV} \sim m_W$

This section outlines the approach of adding $Z \to e^\pm\mu^\mp$ to the observables, and removing the contribution of the flavour-changing Z penguin from the four-fermion operators. This ensures that the basis vectors are orthogonal at m_W to within a degree or two, and highlights the importance of $Z \to e^\pm\mu^\mp$ for distinguishing among coefficients and models.

The operators $\mathcal{O}_{HL1}^{e\mu}$ and $\mathcal{O}_{HL3}^{e\mu}$ of Eq. (C.1) mediate flavour-changing Z decays, upon which ATLAS [79] sets the constraint $BR(Z \to e^\pm\mu^\mp) < 7.5 \times 10^{-7}$ (based on 20 fb^{-1} of luminosity), implying:

$$\frac{v^2}{\Lambda_{LFV}^2}|C_{HL1}^{e\mu} + C_{HL3}^{e\mu}| \lesssim 1.6 \times 10^{-3} \qquad \text{(C.4)}$$

The current sensitivity of $\mu A \to eA$ and $\mu \to e\bar{e}e$ to these coefficients is three orders of magnitude better, and should improve by another two orders of magnitude with upcoming experiments. Nonetheless, improving the experimental reach in $Z \to e^\pm\mu^\mp$ is interesting, because experiments at muon mass scale cannot distinguish these penguin operators from the four-fermion ones.[6]

We include an additional basis vector in the coefficient subspace above m_W:

$$\hat{e}_{ping} = \frac{1}{\sqrt{2}}(\hat{e}_{HL1} + \hat{e}_{HL3}) \qquad \text{(C.5)}$$

(for the case of an outgoing e_L; for outgoing e_R it would be $\hat{e}_{HE}$), and rewrite the operator coefficients in spherical coordinates as

$$\vec{C} = \frac{1}{\Lambda_{LFV}^2}\left[\cos\theta_{ping}\hat{e}_{ping} + \sin\theta_{ping}\cos\theta_D\hat{e}_D\right.$$
$$+ \sin\theta_{ping}\sin\theta_D\cos\theta_S\hat{e}_{S,R}$$
$$+ \sin\theta_{ping}\sin\theta_D\sin\theta_S\cos\theta_{VR}\hat{e}_{V,R}$$
$$+ \sin\theta_{ping}\sin\theta_D\sin\theta_S\sin\theta_{VR}\cos\theta_{VL}\hat{e}_{V,L}$$
$$\left. + \sin\theta_{ping}\sin\theta_D\sin\theta_S\sin\theta_{VR}\sin\theta_{VL}(\sin\phi\hat{e}_{Al} + \cos\phi\hat{e}_\perp)\right],$$
$$\text{(C.6)}$$

where $\theta_J : 0..\pi$ and $\phi : 0..2\pi$, and recall that a model would predict the various angles and the scale.

The expressions for low energy BRs in this enlarged basis become more complicated, because the low energy four-fermion coefficients are expressed as the component from Z exchange, plus the component from four-fermion operator at the weak scale. The normalisation of some basis vectors changes as well, becoming:

---

[6] The situations of the Z-penguin and the dipole are rather different: the dipole is far better constrained than the penguin, because its easier to produce muons than Z bosons. However, the dipole is also constrained by $BR(\mu \to e\bar{e}e)$, and could be distinguished from four-fermion operators using angular distributions in $\mu \to e\bar{e}e$, whereas $Z \to e^\pm\mu^\mp$ appears crucial for constraining and identifying the penguins.

$|e_{VL}| = 0.944$, $|e_{VR}| = 1.041$, $|e_{Al}| = 0.768$, $|e_{Aheavy\perp}|$
$= 0.861$ \hfill (C.7)

The formulae for the reach, obtained from the Branching Ratios are:

$$\frac{\Lambda}{v} = \left[\frac{384\pi^2}{\text{BR}(\mu \to e_L\gamma)} \right]^{1/4}$$
$$\times \sqrt{(|\vec{e}_D|\sin\theta_{ping}\cos\theta_D + 1.21 \times 10^{-3}\cos\theta_{ping})^2}$$
\hfill (C.8)

where the one-loop matching of penguin operators to the dipole was included. For $\mu \to e\bar{e}e$:

$$\frac{\Lambda}{v} = \left[\frac{1}{\text{BR}(\mu \to e\bar{e}e)} \right]^{1/4} \sqrt{\frac{|\vec{e}_S|\sin\theta_{ping}\sin\theta_D\cos\theta_S}{2\sqrt{2}}}$$

$$\frac{\Lambda}{v} = \left[\frac{1}{\text{BR}(\mu \to e\bar{e}e)} \right]^{1/4}$$
$$\times \left[(|\vec{e}_{VR}|\sin\theta_{ping}\sin\theta_D\sin\theta_S\cos\theta_{VR} \right.$$
$$+ 0.685\cos\theta_{ping} + 4e|\vec{e}_D|\sin\theta_{ping}\cos\theta_D)^2$$
$$\left. + 9.38(|\vec{e}_D|\sin\theta_{ping}\cos\theta_D)^2 \right]^{1/4}$$

$$\frac{\Lambda}{v} = \left[\frac{1}{\text{BR}(\mu \to e\bar{e}e)} \right]^{1/4}$$
$$\times \left[2(|\vec{e}_{VL}|\sin\theta_{ping}\sin\theta_D\sin\theta_S\sin\theta_{VR}\cos\theta_{VL} \right.$$
$$- 0.722\cos\theta_{ping} + 4e|\vec{e}_D|\sin\theta_{ping}\cos\theta_D)^2$$
$$\left. + 9.38(|\vec{e}_D|\sin\theta_{ping}\cos\theta_D)^2 \right]^{1/4}$$
\hfill (C.9)

where 0.685 and -0.722 correspond respectively to $\sqrt{2}g^e_{R,L}$ $\times$QED loop corrections. Finally, subtracting the penguins from the u and d vector operators in $\mu A \to eA$ gives

$$\frac{\Lambda}{v} = \left[\frac{1.2292 \times 10^5}{\text{BR}(\mu Al \to eAl)} \right]^{1/4}$$
$$\times \left[|\vec{u}_{Al}|(|\vec{e}_{Al}|\sin\theta_{ping}\sin\theta_D\sin\theta_S \right.$$
$$\sin\theta_{VR}\sin\theta_{VL}\sin\phi - 0.0263\cos\theta_{ping})$$
$$\left. + \frac{D_{Al}}{4}|\vec{e}_D|\sin\theta_{ping}\cos\theta_D \right]^{1/2}$$

$$\frac{\Lambda}{v} = \left[\frac{6.63435 \times 10^3}{\text{BR}(\mu Au \to eAu)} \right]^{1/4}$$
$$\times \left[|\vec{u}_{Au}|(\cos\theta_{AuAl}|\vec{e}_{Al}|\sin\theta_{ping}\sin\theta_D\sin\theta_S\sin\theta_{VR} \right.$$
$$\times \sin\theta_{VL}\sin\phi + \sin\theta_{AuAl}|\vec{e}_\perp|\sin\theta_{ping}\sin\theta_D\sin\theta_S$$
$$\times \sin\theta_{VR}\sin\theta_{VL}\cos\phi - 0.0474\cos\theta_{ping})$$
$$\left. + \frac{D_{Au}}{4}|\vec{e}_D|\sin\theta_{ping}\cos\theta_D \right]^{1/2}$$
\hfill (C.10)

C3. The eigenbasis of the covariance matrix

An alternative basis for the subspace of constrained coefficients, also orthogonal and perhaps more familiar, would be the eigenvectors of the covariance matrix. The inverse covariance matrix V for all the processes can be written as

$$\vec{C}^\dagger V \vec{C} = \vec{C}^\dagger \frac{R_{\mu\to e\gamma}}{B^{expt}_{\mu\to e\gamma}} \vec{C} + \vec{C}^\dagger \frac{R_{\mu\to e\bar{e}e}}{B^{expt}_{\mu\to e\bar{e}e}} \vec{C} + \vec{C}^\dagger \frac{R_{\mu Al\to eAl}}{B^{expt}_{\mu Al\to eAl}} \vec{C}$$
$$+ \vec{C}^\dagger \frac{R_{\mu Au\to eAu}}{B^{expt}_{\mu Au\to eAu}} \vec{C},$$
\hfill (C.11)

where the coefficients are evaluated at the experimental scale. The inverse eigenvalues give the allowed range of coefficients in the eigenbasis, and the eigenvectors are orthogonal combinations of operators, which correspond to the axes of the allowed ellipse around the origin in coefficient space. This is a convenient basis for plotting, because the limiting values of each parameter are obtained on the axes, so there is no need to do perform scans. However, we prefer the operator basis of Eq. (2.1), because it is simple and directly related to the experimental processes.

A covariance matrix for the coefficients at Λ_{LFV} can be obtained by substituting Eq. (2.7) into Eq. (C.11). This matrix is large, ($\sim 90 \times 90$), so despite that most of the eigenvalues should vanish, finding the eigenvectors of the 12 non-zero eigenvalues would be a numerical exercise which could disconnect the final basis and constraints from the input processes. It has the advantage of giving an *orthonormal* basis, whose eigenvectors correspond to the axes of the allowed ellipse in coefficient space.

References

1. Y. Kuno, Y. Okada, Muon decay and physics beyond the standard model. Rev. Mod. Phys. **73**, 151–202 (2001). https://doi.org/10.1103/RevModPhys.73.151. arXiv:hep-ph/9909265
2. L. Calibbi, G. Signorelli, Charged lepton flavour violation: an experimental and theoretical introduction. Riv. Nuovo Cim. **41**(2), 71–174 (2018). https://doi.org/10.1393/ncr/i2018-10144-0. arXiv:1709.00294 [hep-ph]
3. M.C. Gonzalez-Garcia, Y. Nir, Neutrino masses and mixing: evidence and implications. Rev. Mod. Phys. **75**, 345–402 (2003). https://doi.org/10.1103/RevModPhys.75.345. arXiv:hep-ph/0202058
4. M. Fukugita, T. Yanagida, Baryogenesis without grand unification. Phys. Lett. B **174**, 45–47 (1986). https://doi.org/10.1016/0370-2693(86)91126-3
5. S. Davidson, E. Nardi, Y. Nir, Leptogenesis. Phys. Rep. **466**, 105–177 (2008). https://doi.org/10.1016/j.physrep.2008.06.002. arXiv:0802.2962 [hep-ph]
6. A.M. Baldini et al. [MEG Collaboration], Search for the lepton flavour violating decay $\mu^+ \to e^+\gamma$ with the full dataset of the MEG experiment. Eur. Phys. J. C **76**(8), 434 (2016). https://doi.org/10.1140/epjc/s10052-016-4271-x. arXiv:1605.05081 [hep-ex]
7. A.M. Baldini et al. [MEG II Collaboration], The design of the MEG II experiment. Eur. Phys. J. C **78**(5), 380 (2018). https://doi.org/10.

1140/epjc/s10052-018-5845-6. arXiv:1801.04688 [physics.ins-det]

8. U. Bellgardt et al. [SINDRUM Collaboration], Search for the decay mu+ -> e+ e+ e-. Nucl. Phys. B **299**, 1 (1988). https://doi.org/10.1016/0550-3213(88)90462-2

9. A. Blondel et al., Research proposal for an experiment to search for the decay $\mu \to eee$. arXiv:1301.6113 [physics.ins-det]

10. W.H. Bertl et al. [SINDRUM II Collaboration], A search for muon to electron conversion in muonic gold. Eur. Phys. J. C **47**, 337 (2006). https://doi.org/10.1140/epjc/s2006-02582-x

11. C. Dohmen et al. [SINDRUM II Collaboration], Test of lepton flavor conservation in mu -> e conversion on titanium. Phys. Lett. B **317**, 631 (1993)

12. Y.G. Cui et al. [COMET Collaboration], Conceptual design report for experimental search for lepton flavor violating mu−−e− conversion at sensitivity of $10^{**}(−16)$ with a slow-extracted bunched proton beam (COMET), KEK-2009-10

13. M.L. Wong [COMET Collaboration], Overview of the COMET Phase-I experiment. PoS FPCP **2015**, 059 (2015)

14. R.M. Carey et al. [Mu2e Collaboration], Proposal to search for $\mu^- N \to e^- N$ with a single event sensitivity below 10^{-16}, FERMILAB-PROPOSAL-0973

15. Y. Kuno et al. [PRISM collaboration], An experimental search for a $\mu N \to eN$ conversion at sensitivity of the order of 10^{-18} with a highly intense muon source: PRISM, unpublished, J-PARC LOI (2006)

16. B. Aubert et al., Searches for lepton flavor violation in the decays tau+→ e+- gamma and tau+ → mu+- gamma. Phys. Rev. Lett. **104**, 021802 (2010)

17. W. Altmannshofer et al., The Belle II Physics Book. PTEP **2019**(12), 123C01 (2019) [Erratum: PTEP 2020, 029201 (2020)]

18. K. Hayasaka et al., Search for lepton flavor violating tau decays into three leptons with 719 million produced tau+tau− pairs. Phys. Lett. B **687**, 139–143 (2010)

19. Y. Miyazaki et al., Search for lepton flavor violating tau- decays into l- eta, l- eta-prime and l- pi0. Phys. Lett. B **648**, 341–350 (2007)

20. J. Hisano, T. Moroi, K. Tobe, M. Yamaguchi, Lepton flavor violation via right-handed neutrino Yukawa couplings in supersymmetric standard model. Phys. Rev. D **53**, 2442–2459 (1996). https://doi.org/10.1103/PhysRevD.53.2442. arXiv:hep-ph/9510309

21. W. Altmannshofer, A.J. Buras, S. Gori, P. Paradisi, D.M. Straub, Anatomy and phenomenology of FCNC and CPV effects in SUSY theories. Nucl. Phys. B **830**, 17–94 (2010). https://doi.org/10.1016/j.nuclphysb.2009.12.019. arXiv:0909.1333 [hep-ph]

22. M. Blanke, A.J. Buras, B. Duling, A. Poschenrieder, C. Tarantino, Charged lepton flavour violation and (g-2)(mu) in the littlest Higgs model with T-parity: a clear distinction from supersymmetry. JHEP **05**, 013 (2007). https://doi.org/10.1088/1126-6708/2007/05/013. arXiv:hep-ph/0702136 [hep-ph]

23. Y. Omura, E. Senaha, K. Tobe, Lepton-flavor-violating Higgs decay $h \to \mu\tau$ and muon anomalous magnetic moment in a general two Higgs doublet model. JHEP **05**, 028 (2015). https://doi.org/10.1007/JHEP05(2015)028. arXiv:1502.07824 [hep-ph]

24. E. Arganda, M.J. Herrero, X. Marcano, C. Weiland, Imprints of massive inverse seesaw model neutrinos in lepton flavor violating Higgs boson decays. Phys. Rev. D **91**(1), 015001 (2015). https://doi.org/10.1103/PhysRevD.91.015001. arXiv:1405.4300 [hep-ph]

25. F. Deppisch, J.W.F. Valle, Enhanced lepton flavor violation in the supersymmetric inverse seesaw model. Phys. Rev. D **72**, 036001 (2005). https://doi.org/10.1103/PhysRevD.72.036001. arXiv:hep-ph/0406040

26. S. Antusch, E. Arganda, M.J. Herrero, A.M. Teixeira, Impact of theta(13) on lepton flavour violating processes within SUSY seesaw. JHEP **11**, 090 (2006). https://doi.org/10.1088/1126-6708/2006/11/090. arXiv:hep-ph/0607263 [hep-ph]

27. T.M. Aliev, A.S. Cornell, N. Gaur, Lepton flavour violation in unparticle physics. Phys. Lett. B **657**, 77–80 (2007). https://doi.org/10.1016/j.physletb.2007.09.055. arXiv:0705.1326 [hep-ph]

28. M.L. López-Ibáñez, A. Melis, M.J. Pérez, M.H. Rahat, O. Vives, Constraining low-scale flavor models with $(g-2)\mu$ and lepton flavor violation. Phys. Rev. D **105**(3), 035021 (2022). https://doi.org/10.1103/PhysRevD.105.035021. arXiv:2112.11455 [hep-ph]

29. P. Escribano, M. Hirsch, J. Nava, A. Vicente, Observable flavor violation from spontaneous lepton number breaking. JHEP **01**, 098 (2022). https://doi.org/10.1007/JHEP01(2022)098. arXiv:2108.01101 [hep-ph]

30. Y. Cai, J. Herrero-García, M.A. Schmidt, A. Vicente, R.R. Volkas, From the trees to the forest: a review of radiative neutrino mass models. Front. Phys. **5**, 63 (2017). https://doi.org/10.3389/fphy.2017.00063. arXiv:1706.08524 [hep-ph]

31. A. de Gouvea, P. Vogel, Lepton flavor and number conservation, and physics beyond the standard model. Prog. Part. Nucl. Phys. **71**, 75–92 (2013). https://doi.org/10.1016/j.ppnp.2013.03.006. arXiv:1303.4097 [hep-ph]

32. A. Crivellin, S. Davidson, G.M. Pruna, A. Signer, Renormalisation-group improved analysis of $\mu \to e$ processes in a systematic effective-field-theory approach. JHEP **05**, 117 (2017). arXiv:1702.03020 [hep-ph]

33. S. Davidson, Completeness and complementarity for $\mu \to e\gamma \mu \to e\bar{e}e$ and $\mu A \to eA$. JHEP **02**, 172 (2021). https://doi.org/10.1007/JHEP02(2021)172. arXiv:2010.00317 [hep-ph]

34. H. Georgi, Effective field theory. Annu. Rev. Nucl. Part. Sci. **43**, 209–252 (1993)

35. H. Georgi, On-shell effective field theory. Nucl. Phys. B **361**, 339–350 (1991)

36. A.J. Buras, Weak Hamiltonian, CP violation and rare decays. arXiv:hep-ph/9806471

37. L. Houches, Lect. Notes **108** (2020)

38. A.V. Manohar, Introduction to effective field theories. arXiv:1804.05863 [hep-ph]

39. A. Pich, Effective field theory with Nambu–Goldstone modes. arXiv:1804.05664 [hep-ph]

40. L. Silvestrini, Effective theories for quark flavour physics. arXiv:1905.00798 [hep-ph]

41. M. Balsiger, M. Bounakis, M. Drissi, J. Gargalionis, E. Gustafson, G. Jackson, M. Leak, C. Lepenik, S. Melville, D. Moreno et al., Solutions to problems at Les Houches Summer School on EFT. arXiv:2005.08573 [hep-ph]

42. S. Davidson, Y. Kuno, M. Yamanaka, Selecting $\mu \to e$ conversion targets to distinguish lepton flavour-changing operators. Phys. Lett. B **790**, 380 (2019). https://doi.org/10.1016/j.physletb.2019.01.042. arXiv:1810.01884 [hep-ph]

43. R. Alonso, E.E. Jenkins, A.V. Manohar, M. Trott, Renormalization group evolution of the standard model dimension six operators III: gauge coupling dependence and phenomenology. JHEP **1404**, 159 (2014). arXiv:1312.2014 [hep-ph]

44. E.E. Jenkins, A.V. Manohar, M. Trott, Renormalization group evolution of the standard model dimension six operators II: Yukawa dependence. JHEP **1401**, 035 (2014). https://doi.org/10.1007/JHEP01(2014)035. arXiv:1310.4838 [hep-ph]

45. V. Cirigliano, S. Davidson, Y. Kuno, Spin-dependent $\mu \to e$ conversion. Phys. Lett. B **771**, 242 (2017). https://doi.org/10.1016/j.physletb.2017.05.053. arXiv:1703.02057 [hep-ph]

46. S. Davidson, Y. Kuno, A. Saporta, Spin-dependent $\mu \to e$ conversion on light nuclei. Eur. Phys. J. C **78**(2), 109 (2018). https://doi.org/10.1140/epjc/s10052-018-5584-8. arXiv:1710.06787 [hep-ph]

47. M. Ciuchini, E. Franco, L. Reina and L. Silvestrini, Leading order QCD corrections to b → s gamma and b → s g decays in three regularization schemes. Nucl. Phys. B **421**, 41 (1994). arXiv:hep-ph/9311357

48. W. Christopher, Murphy, dimension-8 operators in the standard model effective field theory. JHEP **10**, 174 (2020)

49. H.-L. Li, Z. Ren, J. Shu, M.-L. Xiao, Y. Jiang-Hao, Y.-H. Zheng, Complete set of dimension-eight operators in the standard model effective field theory. Phys. Rev. D **104**(1), 015026 (2021)

50. M. Ardu, S. Davidson, What is leading order for LFV in SMEFT? JHEP **08**, 002 (2021). https://doi.org/10.1007/JHEP08(2021)002. arXiv:2103.07212 [hep-ph]

51. L.E. Blumenson, A derivation of n-dimensional spherical coordinates. Am. Math. Mon. **67**(1), 63–66 (1960). http://www.jstor.org/stable/2308932

52. Y. Okada, K.I. Okumura, Y. Shimizu, Mu → e gamma and mu → 3 e processes with polarized muons and supersymmetric grand unified theories. Phys. Rev. D **61**, 094001 (2000). https://doi.org/10.1103/PhysRevD.61.094001. arXiv:hep-ph/9906446

53. Y. Okada, K.I. Okumura, Y. Shimizu, CP violation in the mu → 3 e process and supersymmetric grand unified theory. Phys. Rev. D **58**, 051901 (1998). https://doi.org/10.1103/PhysRevD.58.051901. arXiv:hep-ph/9708446

54. J. Hisano, T. Moroi, K. Tobe, M. Yamaguchi, Exact event rates of lepton flavor violating processes in supersymmetric SU(5) model. Phys. Lett. B **391**, 341–350 (1997) [Erratum: Phys. Lett. B **397**, 357 (1997)] .https://doi.org/10.1016/S0370-2693(96)01473-6. arXiv:hep-ph/9605296

55. S. Davidson, D.C. Bailey, B.A. Campbell, Model independent constraints on leptoquarks from rare processes. Z. Phys. C **61**, 613–644 (1994). https://doi.org/10.1007/BF01552629. [arXiv:hep-ph/9309310 [hep-ph]]

56. I. Doršner, S. Fajfer, A. Greljo, J.F. Kamenik, N. Košnik, Physics of leptoquarks in precision experiments and at particle colliders. Phys. Rep. **641**, 1–68 (2016). https://doi.org/10.1016/j.physrep.2016.06.001. arXiv:1603.04993 [hep-ph]

57. V. Cirigliano, M.L. Graesser, G. Ovanesyan, WIMP-nucleus scattering in chiral effective theory. JHEP **10**, 025 (2012). https://doi.org/10.1007/JHEP10(2012)025. arXiv:1205.2695 [hep-ph]

58. M. Hoferichter, P. Klos, A. Schwenk, Chiral power counting of one- and two-body currents in direct detection of dark matter. Phys. Lett. B **746**, 410–416 (2015). https://doi.org/10.1016/j.physletb.2015.05.041. arXiv:1503.04811 [hep-ph]

59. A. Crivellin, M. Hoferichter, M. Procura, Improved predictions for $\mu \to e$ conversion in nuclei and Higgs-induced lepton flavor violation. Phys. Rev. D **89**, 093024 (2014). https://doi.org/10.1103/PhysRevD.89.093024. arXiv:1404.7134 [hep-ph]

60. V. Cirigliano, K. Fuyuto, M.J. Ramsey-Musolf, E. Rule, Next-to-leading order scalar contributions to $\mu \to e$ conversion. arXiv:2203.09547 [hep-ph]

61. W. Dekens, E.E. Jenkins, A.V. Manohar, P. Stoffer, Non-perturbative effects in $\mu \to e\gamma$. JHEP **01**, 088 (2019). https://doi.org/10.1007/JHEP01(2019)088. arXiv:1810.05675 [hep-ph]

62. R. Kitano, M. Koike, Y. Okada, Detailed calculation of lepton flavor violating muon electron conversion rate for various nuclei. Phys. Rev. D **66**, 096002 (2002) [Erratum: Phys. Rev. D **76**, 059902 (2007)]. https://doi.org/10.1103/PhysRevD.76.059902. arXiv:hep-ph/0203110

63. S. Borsanyi, Z. Fodor, C. Hoelbling, L. Lellouch, K.K. Szabo, C. Torrero, L. Varnhorst, Ab-initio calculation of the proton and the neutron's scalar couplings for new physics searches. arXiv:2007.03319 [hep-lat]

64. M. Hoferichter, J. Ruiz de Elvira, B. Kubis, U.G. Meissner, High-precision determination of the pion-nucleon term from Roy–Steiner equations. Phys. Rev. Lett. **115**, 092301 (2015). https://doi.org/10.1103/PhysRevLett.115.092301. arXiv:1506.04142 [hep-ph]

65. A. Crivellin, M. Hoferichter, M. Procura, Accurate evaluation of hadronic uncertainties in spin-independent WIMP-nucleon scattering: disentangling two- and three-flavor effects. Phys. Rev. D **89**, 054021 (2014). https://doi.org/10.1103/PhysRevD.89.054021. arXiv:1312.4951 [hep-ph]

66. J. Ruiz de Elvira, M. Hoferichter, B. Kubis, U.G. Meißner, Extracting the σ-term from low-energy pion-nucleon scattering. J. Phys. G **45**(2), 024001 (2018). https://doi.org/10.1088/1361-6471/aa9422. arXiv:1706.01465 [hep-ph]

67. S. Durr et al., Lattice computation of the nucleon scalar quark contents at the physical point. Phys. Rev. Lett. **116**(17), 172001 (2016). https://doi.org/10.1103/PhysRevLett.116.172001. arXiv:1510.08013 [hep-lat]

68. P. Junnarkar, A. Walker-Loud, Scalar strange content of the nucleon from lattice QCD. Phys. Rev. D **87**, 114510 (2013). https://doi.org/10.1103/PhysRevD.87.114510. arXiv:1301.1114 [hep-lat]

69. J.M. Alarcon, J. Martin Camalich, J.A. Oller, The chiral representation of the πN scattering amplitude and the pion-nucleon sigma term. Phys. Rev. D **85**, 051503 (2012). https://doi.org/10.1103/PhysRevD.85.051503. arXiv:1110.3797 [hep-ph]

70. R. Gupta, S. Park, M. Hoferichter, E. Mereghetti, B. Yoon, T. Bhattacharya, Pion-nucleon sigma term from lattice QCD. Phys. Rev. Lett. **127**(24), 24 (2021). https://doi.org/10.1103/PhysRevLett.127.242002. arXiv:2105.12095 [hep-lat]

71. M.A. Shifman, A.I. Vainshtein, V.I. Zakharov, Remarks on Higgs boson interactions with nucleons. Phys. Lett. B **78**, 443 (1978)

72. K.A. Olive et al. [Particle Data Group], Review of particle physics. Chin. Phys. C **38**, 090001 (2014). https://doi.org/10.1088/1674-1137/38/9/090001

73. P.A. Zyla et al. [Particle Data Group], Review of particle physics. PTEP **2020**(8), 083C01 (2020)

74. S. Davidson, Y. Kuno, M. Yamanaka, Probing $\mu e\gamma\gamma$ contact interactions with $\mu \to e$ conversion. Phys. Rev. D **102**(11), 115043 (2020). arXiv:2007.09612 [hep-ph]

75. T. Suzuki, D.F. Measday, J.P. Roalsvig, Total nuclear capture rates for negative muons. Phys. Rev. C **35**, 2212 (1987). https://doi.org/10.1103/PhysRevC.35.2212

76. V. Cirigliano, R. Kitano, Y. Okada, P. Tuzon, On the model discriminating power of mu -> e conversion in nuclei. Phys. Rev. D **80**, 013002 (2009). https://doi.org/10.1103/PhysRevD.80.013002. arXiv:0904.0957 [hep-ph]

77. W. Buchmuller, D. Wyler, Effective Lagrangian analysis of new interactions and flavor conservation. Nucl. Phys. B **268**, 621 (1986). https://doi.org/10.1016/0550-3213(86)90262-2

78. B. Grzadkowski, M. Iskrzynski, M. Misiak, J. Rosiek, Dimension-six terms in the standard model Lagrangian. JHEP **1010**, 085 (2010). arXiv:1008.4884 [hep-ph]

79. G. Aad et al., [ATLAS], Search for the lepton flavor violating decay $Z \to e\bar{\mu}$ in pp collisions at $\sqrt{s}$ TeV with the ATLAS detector. Phys. Rev. D **90**(7), 072010 (2014). https://doi.org/10.1103/PhysRevD.90.072010. arXiv:1408.5774 [hep-ex]